1978

Deuterium Lamb shift via quenching-radiation anisotropy measurements

A. Van Wijngaarden

Gordon W. F. Drake
University of Windsor

PHYSICAL REVIEW A VOLUME 17, NUMBER 4 APRIL 1978

Deuterium Lamb shift via quenching-radiation anisotropy measurements

A. van Wijngaarden and G. W. F. Drake
Department of Physics, University of Windsor, Windsor, Ontario, Canada N9B3P4
(Received 10 November 1977)

The Lamb shift of a hydrogenic ion can be deduced from the anisotropy in the angular distribution of the $2s_{1/2}$-$1s_{1/2}$ electric field quenching radiation. The accuracy of our previous anisotropy measurement for deuterium is improved to about ± 150 ppm. The derived Lamb shift is (1059.36 ± 0.16) MHz. The sources of error are carefully analyzed and the prospects for further improvements in the accuracy are discussed.

I. INTRODUCTION

The purpose of this paper is to report further progress in a program[1] to develop an alternative method of measuring the $2s_{1/2}$-$2p_{1/2}$ Lamb shift in hydrogen and hydrogenic ions. The method is based on the observation[2] that when a hydrogenic atom in the metastable $2s_{1/2}$ state is quenched by an electric field, the induced Lyman-α (Ly-α) radiation intensity possesses an anisotropy in its angular distribution which is (nearly) proportional to the Lamb shift. The complete angular distribution pattern need not be measured—only the ratio $I_{\parallel}/I_{\perp}$ of the intensities emitted parallel and perpendicular to the applied field direction. The corresponding anisotropy $R = (I_{\parallel} - I_{\perp})/(I_{\parallel} + I_{\perp})$ is a maximum for these two directions.

We have demonstrated previously[1] that the anisotropy for H and D can be measured to an accuracy of ±0.1%. In this paper, the accuracy for D is improved by about an order of magnitude to ±0.014% (±140 ppm). We use D rather than H because time-dependent effects resulting from hyperfine structure[1] are smaller.

There are several reasons why a measurement of improved accuracy is of interest. First, the method can be extended in a straightforward way to the heavy hydrogenic ions. No other technique (such as quench-rate measurements[3-7] or laser resonance measurements[8,9]) presently offers comparable accuracy in the range $3 \leq Z \leq 10$. It is therefore important to verify that all phenomena are thoroughly understood for an atom such as D, where the Lamb shift is already accurately known (±60 ppm). Lamb shift measurements in hydrogenic ions have recently been reviewed by Kugel and Murnick.[10] Second, the present measurement provides a precise test of theories describing the time-dependent interaction between atoms and external electric fields. Third, the prospects are good that the accuracy can be improved still further, making the anisotropy method competitive with microwave resonance techniques[11-15] for H, D, and He^+. The separated-oscillatory-fields measurement of Lundeen and Pipkin[15] for H is accurate to ±20 ppm; other resonance-type measurements are accurate to ±60 ppm for H (Refs. 11 and 12) and D (Refs. 11 and 13), and ±90 ppm for He^+ (Ref. 14).

The remainder of the paper is divided into the following sections: The experimental apparatus and procedure is discussed in Sec. II, followed by a description of the theory used to interpret the results in Sec. III. The experimental results are presented in Sec. IV, together with a careful analysis of the measurement statistics. The statistical analysis of our large number of data points is an interesting study in itself. The systematic corrections are discussed in Sec. V, and the final results presented in Sec. VI. We discuss here also the problems associated with further improvements in the accuracy of such measurements.

II. EXPERIMENTAL APPARATUS AND PROCEDURE

A. Description of the experiment

A schematic diagram of the apparatus is shown in Fig. 1. The experiment is basically the same as the one described previously,[1] but a number of modifications have been made to improve the accuracy. Briefly, a deuterium beam containing a large fraction of metastable atoms is formed by passing 6.36-KeV D^+ ions through a cell containing Cs vapor. To reduce background noise, a small electric field (~6 V/cm) is applied between the prequenching plates to remove charged particles from the beam. The remaining beam is collimated and then enters the quadrupole quenching field region. Here, the induced photons emitted in two perpendicular directions are counted simultaneously by a double-counter system, and the beam current is recorded by a neutral-particle detector. Simultaneous counting is essential in a precision experiment to avoid systematic errors due to beam fluctuations.

In the present experiment, all the data are taken at a single field strength of about 82 V/cm, rather than using a range of field strengths and extrapo-

lating to zero as in our previous work. Since random fluctuations in the counting statistics are the dominant source of error, this strategy gives the greatest possible statistical accuracy while avoiding the errors inherent in taking data at very low field strengths (such as low counting rate, stray fields, contact potentials, etc.). The disadvantage is that the field strength along the beam axis must be accurately known in order to calculate reliably the time-dependent anisotropy at finite field strengths.

A new quadrupole system (see Fig. 1) was therefore precision machined to a tolerance of ±0.005 mm in all critical dimensions. The field at the beam axis is produced by connecting together the rods in two nearest-neighbor pairs with the pairs held at opposite potentials. The rods are enclosed in a box of square cross section held at ground potential to provide a well-defined boundary condition for the field inside. The end plates with small entrance and exit apertures are also grounded. The quadrupole rods 1.016 cm in diameter and 10.7 cm long are located on a circle of diameter 4.572 cm. The outer box is 9.65 cm on each side and 10.7 cm long.

The ultraviolet photon detectors (Galileo Electro-Optics model BX762) have a quantum efficiency of about 10% for Ly-α radiation.

B. Electric field calculation

The calculation of the electric field near the beam axis is in principle straightforward, but since the results must be accurate to ±0.1% or better for our somewhat complicated three-dimensional geometry, the computational problems are not trivial. The methods used will therefore be described in some detail.

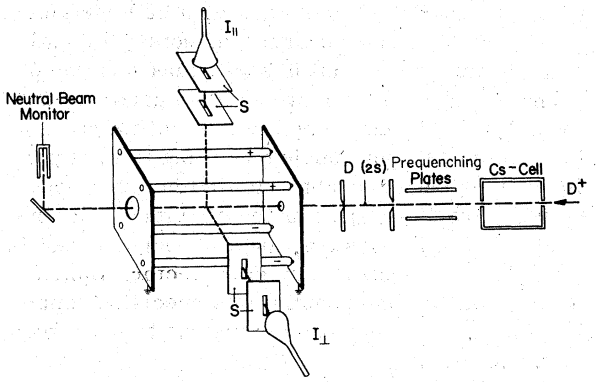

FIG. 1. Schematic diagram of the apparatus. Not shown is an outer grounded box of square cross section in which the inner pair of slits is mounted. $I_{\parallel}$ and $I_{\perp}$ are the measured intensities when the quenching rods are held at potentials $V(+)$ and $-V(-)$ are shown.

The problem is to solve the Laplace equation

$$\nabla^2\Phi = 0 \tag{1}$$

for the electric potential Φ, subject to the boundary conditions that all surfaces are grounded except for the quadrupole rods which are held at potentials V and $-V$ in nearest-neighbor pairs. The solution is built up in three steps. The first step is to solve the modified problem in which the length of the cell and the cross-sectional size of the outer box are assumed to be infinite. The effects of finite box width and length are then small corrections, at least in the observation region near the center of the cell. The exact solution to the above modified problem can be expanded in the form

$$\Phi_0 = \begin{cases} \sum_{n=0}^{\infty} A_n \rho^{2n+1} \sin(2n+1)\theta, & \rho \le R \\ \sum_{n=0}^{\infty} A_n \left(\frac{R^2}{\rho}\right)^{2n+1} \sin(2n+1)\theta, & \rho > R, \end{cases} \tag{2}$$

where $R = (2a^2 - b^2)^{1/2}$ (see Fig. 2) is the radius of the circle of inversion symmetry; i.e., the problem is invariant under the transformation $\rho \to R^2/\rho$. Each term of (2) individually satisfies (1). The coefficients A_n are determined by the boundary conditions in the first quadrant:

$$\Phi_0[\rho(\theta), \theta] = V, \quad \theta_1 \le \theta \le \theta_2 \tag{3}$$

$$\left.\frac{\partial\Phi_0(\rho, \theta)}{\partial\rho}\right|_{\rho = R} = 0, \quad 0 \le \theta < \theta_1 \text{ and } \theta_2 < \theta \le \tfrac{1}{2}\pi \tag{4}$$

where

$$\theta_1 = \tfrac{1}{2}\sin^{-1}(1 - b^2/a^2), \qquad \theta_2 = \tfrac{1}{2}\pi - \theta_1 \tag{5}$$

are the values of θ for the two radial lines which are tangent to the rod (see Fig. 2),

$$\rho(\theta) = \sqrt{2}\, a\cos\beta - (b^2 - 2a^2\sin^2\beta)^{1/2}, \qquad \beta = \tfrac{1}{4}\pi - \theta \tag{6}$$

is the equation of the arc defining the rod surface for $\theta_1 \le \theta \le \theta_2$, and V is the constant potential on the rod. Only the first quadrant need be considered since the symmetry conditions

$$\Phi_0(\rho, 0) = 0$$

and (7)

$$\left.\frac{\partial\Phi_0(\rho, \theta)}{\partial\theta}\right|_{\theta = \frac{1}{2}\pi} = 0$$

are automatically satisfied by (2).

To find the coefficients A_n, the expansion (2) is truncated after the first N terms, and the functional

$$J = c_1 J_1 + c_2 J_2, \tag{8}$$

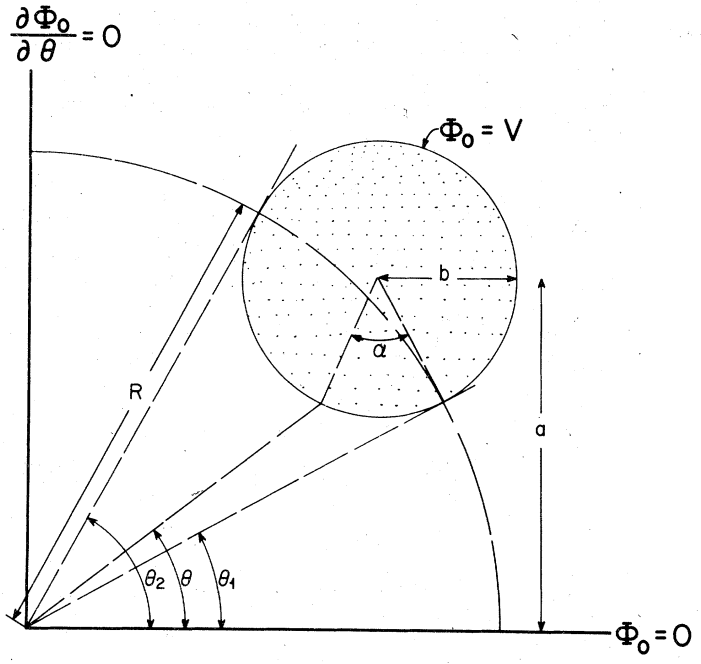

FIG. 2. Cross-sectional view of the first quadrant of the quenching cell, drawn approximately to scale with $a = 1.6165$ cm and $b = 0.5080$ cm. The deuterium beam passes through the origin perpendicular to the page. The boundary conditions on the electric potential shown along the horizontal and vertical axes are imposed by the symmetry of the cell.

where

$$J_1 = \int_{\theta_1}^{\theta_2} \left(\sum_{n=0}^{N} A_n \rho(\theta)^{2n+1} \sin(2n+1)\theta - V \right)^2 \left(\frac{d\alpha}{d\theta} \right) d\theta , \tag{9}$$

$$J_2 = \int_0^{\theta_1} \left(\sum_{n=0}^{N} (2n+1) A_n R^{2n} \sin(2n+1)\theta \right)^2 d\theta + \int_{\theta_2}^{\pi/2} \left(\sum_{n=0}^{N} (2n+1) A_n R^{2n} \sin(2n+1)\theta \right)^2 d\theta , \tag{10}$$

is formed to measure the mean-square deviation of the solution from the boundary conditions (3) and (4). The angle α is the one shown in Fig. 2 and the factor $d\alpha/d\theta$ is included in (9) so that points on the rod surface are weighted equally. The conditions

$$\frac{\partial J}{\partial A_n} = 0, \quad n = 1, 2, \ldots, N \tag{11}$$

then determine N linear equations in N unknowns which are solved for the A_n. The arbitrary weighting factors c_1 and c_2 in (8) can be adjusted to optimize the rate of convergence of the A_n with increasing N. For $N = 40$, the first few A_n's converge to the values

$$A_0 = 0.912\,85 V/a,$$

$$A_1 = 0.193\,63 V/a^3,$$

$$A_2 = -0.039\,83 V/a^5,$$

for our geometry, with $a = 1.6165 \pm 0.0005$ cm.

If we define a coordinate system such that the y axis lies along the beam axis and the z axis points in the dominant field direction, then the electric field components near the beam axis are

$$E_z = -\frac{\partial \Phi_0}{\partial z} = -A_0 - 3A_1(x^2 - z^2) + \cdots ,$$

$$E_x = -\frac{\partial \Phi_0}{\partial x} = -6A_1 xz + \cdots . \tag{12}$$

Since the beam radius is small compared to the dimensions of the quenching cell, the A_1 corrections to the field turn out to be negligible.

The small corrections to A_0 due to the finite box width and quenching-cell length are included by a superposition of solutions. The second step therefore consists of solving the two-dimensional problem with the boundary condition $\Phi_1 = -\Phi_0$ on the walls of the enclosing box, and $\Phi_1 = 0$ on the rods. This is done by the well-known numerical technique of subdividing the area with a square grid and demanding that the potential at each grid point be the average of its neighbors. A relatively coarse 48 $\times$ 48 grid, together with the technique of "deferred approach to the limit,"[16] is sufficient to determine the correction

$$\Delta A_0^{(1)} = (-0.030\,69 \pm 0.000\,03) V/a. \tag{13}$$

The third step is to solve similarly the three-dimensional problem for the finite length correction. Here the boundary conditions are $\Phi_2 = -(\Phi_0 + \Phi_1)$ on the grounded end plates, and $\Phi_2 = 0$ on the rods and outer box. This yields the further correction

$$\Delta A_0^{(2)} = (-0.002\,64 \pm 0.000\,01)V/a, \tag{14}$$

along with the field strength as a function of position along the beam axis. The dependence on position along the beam axis is well approximated by the formula

$$E_z(y) = \begin{cases} E_{z,\max} \dfrac{2\sin(\eta y)}{1+\sin^2(\eta y)}, & \eta y < \frac{1}{2}\pi \\ E_{z,\max}, & \eta y \geq \frac{1}{2}\pi \end{cases} \tag{15}$$

with $\eta = 0.356\ \text{cm}^{-1}$ and

$$E_{z,\max} = A_0 + \Delta A_0^{(1)} + \Delta A_0^{(2)} = 0.879\,52V/a. \tag{16}$$

In this experiment, V is fixed at 150.00 V. The field strength at the center of the cell is then $E_{z,\max} = 81.613 \pm 0.05\ \text{V/cm}$. The uncertainty comes primarily from uncertainties in the dimensions of the quenching cell—particularly the rod diameters.

III. THEORY

We describe in this section the induced Ly-α radiation which is emitted when a beam of metastable D atoms enters an asymptotically constant electric field with an initial fringing field extending over a substantial distance. The experimental conditions are such that field entry is nearly adiabatic, but nonadiabatic corrections are significant. We therefore integrate the full time-dependent Schrödinger equation in the finite basis set of 24 states with $n=2$. These are the hyperfine states $2s_{1/2}$ $(F=\frac{1}{2},\frac{3}{2})$, $2p_{1/2}$ $(F=\frac{1}{2},\frac{3}{2})$ and $2p_{3/2}$ $(F=\frac{3}{2},\frac{5}{2})$, each of which is $(2F+1)$- fold degenerate. All calculations are done in the coupled (l,s,j,I,F,M_F) representation, except that the basis set is prediagonalized with respect to off-diagonal matrix elements of the hyperfine-structure interaction. This weakly mixes the states $2p_{1/2}(F=\frac{3}{2})$ and $2p_{3/2}(F=\frac{3}{2})$, and slightly alters the anisotropy.[17]

The method of solution is basically the same as that described previously.[18] Briefly, the time-dependent Schrödinger equation to be solved in the finite basis set is

$$i\frac{d\vec{a}}{dt} = \underline{U}(t)\vec{a}, \qquad \underline{U}(t) = \underline{E} + F(t)\underline{V}, \tag{17}$$

in atomic units, where $\vec{a}$ is the 24-component column vector of time-dependent state amplitudes, $\underline{E}$ is the diagonal matrix of complex field-free eigenvalues, $\underline{V}$ is the interaction matrix with the external electric field, $F(t)$ is the time-dependent field strength given by

$$F(t) = E_z(vt), \tag{18}$$

v is the beam velocity $(0.780\times10^8\ \text{cm/s})$, and $E_z(y)$ is given by (15). The set of coupled equations (17) is solved numerically by first transforming to the representation of asymptotic field-perturbed states defined by

$$\vec{b}(t) = \underline{A}^T\vec{a}(t), \tag{19}$$

where $\underline{A}$ is the matrix such that $\underline{A}^T[\underline{E}+F(\infty)\underline{V}]\underline{A}$ is diagonal with complex eigenvalues $\bar{E}_j$. A separate solution must be found for the initial condition that the atoms are in each of the six hyperfine $2s_{1/2}$ $(F=\frac{1}{2},\frac{3}{2})$ states at time $t=0$. If these states are labeled by $i=1,\ldots,6$, then

$$\Psi_i(t) = \begin{cases} \Psi_i e^{-i\bar{E}_i t}, & t \leq 0 \\ \sum_{k,j}^{24} \Psi_k A_{kj} b_j^{(i)}(t), & t > 0, \end{cases} \tag{20}$$

where $b_j^{(i)}(t)$ is the solution corresponding to the initial condition $a_j(0) = \delta_{j,i}$. As $F(t)$ approaches its limiting value $F(\infty)$, the coefficients $b_j^{(i)}(t)$ tend to the limit functions

$$b_j^{(i)}(t) \to b_j^{(i)}(\infty)e^{-\bar{E}_j t}. \tag{21}$$

The numerical integration can therefore be stopped when this limiting behavior is reached. The above representation yields less rapidly oscillating solutions in the fringing field region than the $c_j^{(i)}(t)$ representation used in Ref. 18. The two differ by factors of $e^{-i\bar{E}_j t}$.

The field-induced electric dipole transitions to the ground-state manifold (labeled by $f=1,\ldots,6,$) proceed via mixing between the $2s$ and $2p$ states. The transition rate for a given polarization vector $\hat{e}$ is proportional to the quantity

$$I(\hat{e},t) = \sum_{i,f} \left|\langle\Psi_i(t)\left|\hat{e}\cdot\vec{r}\right|\Psi_f\rangle\right|^2, \tag{22}$$

assuming that the incident beam is an incoherent mixture of $2s_{1/2}$ hyperfine states with equal statistical weights. For our geometry with the beam along the y axis and the electric field along the z axis, the theoretical anisotropy uncorrected for the finite solid angle of observation is

$$R(t) = \frac{I(\hat{e}_x,t) - I(\hat{e}_z,t)}{I(\hat{e}_x,t) + 2I(\hat{e}_y,t) + I(\hat{e}_z,t)}. \tag{23}$$

The calculated $R(t)$ is plotted as a function of position along the beam axis in Fig. 3. Although the curve appears to be asymptotically flat, it is in fact slowly increasing at the rate of 2.09×10^{-5} cm^{-1}. The observation region is as shown in the figure. The position of the observation region is such that the absolute intensity of the quenching radiation is approximately a maximum as a func-

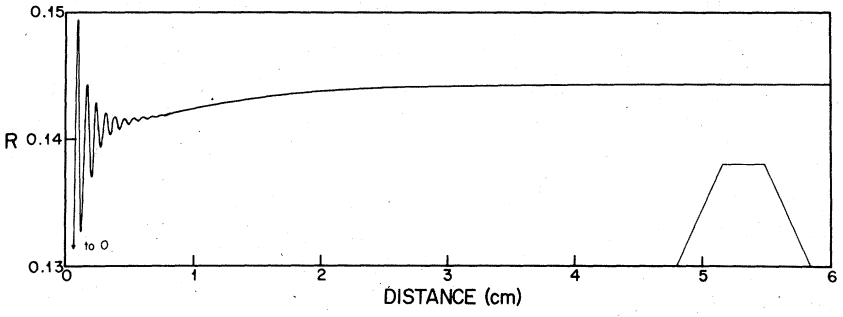

FIG. 3. Calculated anistropy as a function of position along the beam axis. The trapezium to the right is the geometrical slit function of the detector system showing its location along the beam axis.

tion of field strength at our working field of 81.613 V/cm. This reduces errors resulting from changes in absolute intensity due to small variations in field strength either across the beam diameter or as a function of time. Using the input data in Table I, the theoretical value of R at the middle of the observation region is 0.144 245. We also list in Table I the rate of change of R with respect to each of the input parameters.

IV. EXPERIMENTAL DATA AND STATISTICAL ANALYSIS

In all, 2038 individual measurements of R were made, each containing on the average 1.355×10^6 counts. The data were collected in 24 separate runs made on different days. Each measurement consisted of eight counter readings—one for each of the two counters at the four electric field directions obtained by rotating the potentials on the quadrupole rods in steps of 90°. The eight readings were combined into a single measurement as described previously[1] so as to eliminate the relative sensitivities of the two detector systems. The background noise was defined to be the *isotropic* part of the residual signal measured under identical conditions except that most of the metastables in the beam were prequenched before entering the quenching-cell proper. With our signal-to-noise ratio of about 500 : 1, one noise measurement after every five signal measurements was sufficient to make the uncertainty due to noise counting statistics a small correction. The noise corrections to R were typically about 0.2%.

TABLE I. Input data (x) for the theoretical calculation of the D($2s_{1/2}$) quenching anisotropy (R), and sensitivity coefficients (s) [a].

x	Value	s
$E(2s_{1/2})-E(2p_{1/2})$	1059.241 MHz	0.95
$E(2p_{3/2})-E(2p_{1/2})$	10972.02 MHz	−0.95
$\alpha_{\rm HFS}$ [b]	40.923 MHz	<0.0001
$\Gamma(2p)$	6.265×10^8 sec^{-1}	−0.0004
Field strength	81.613 V/cm	0.04
Beam energy	6.355 kV	−0.0004
Distance to observation region	5.33 cm	0.0008
η (Eq. 15)	0.356 cm^{-1}	0.0008

[a] The coefficient s is defined by $\delta R/R = s\delta x/x$, where δR is the change in R induced by a change δx in x.

[b] The hyperfine-structure energy shifts are given by

$$\Delta E_{nljIF}=\frac{\alpha_{\rm HFS}}{n^3}\left(\frac{F(F+1)-j(j+1)-I(I+1)}{j(j+1)(l+\frac{1}{2})}\right).$$

The mean and standard deviation of all the measurements, weighted by the square root of the number of counts in each measurement, are defined by

$$\bar{R}=\sum_{i=1}^{N}R_i n_i^{1/2}\Big/\sum_{i=1}^{N}n_i^{1/2} \tag{24}$$

and

$$\sigma=\left(\sum_{i=1}^{N}\frac{(R_i-\bar{R})^2 n_i}{n_T(N-1)}\right)^{1/2}, \tag{25}$$

where n_i is the number of counts in the ith measurement, n_T is the total number of counts, and N is the number of measurements. The experimental values are

$$\bar{R}=0.144\,087\,9,\quad \sigma=0.000\,019\,9,$$

uncorrected for the finite solid angle of observation and electronic dead time. The theoretically expected standard deviation arising from counting statistics alone is[19]

$$\sigma_R=\tfrac{1}{2}(\alpha^{1/2}+\alpha^{-1/2})[(1-R^2)/n_T]^{1/2}, \tag{26}$$

where α is the ratio of the sensitivities of the two-counter systems. Using $\alpha=0.622$ and $n_T=2.763\times10^9$, the above formula yields $\sigma_R=0.000\,019\,4$. Although this differs by only 3% from the experimental value, the chi-square test shows that the difference is statistically significant at the 98% confidence level. The difference is due to the statistical uncertainty in counting the noise. This effect introduces an additional uncertainty of

$$\sigma_{\rm noise}=\sigma_R F\left(\frac{n_{\rm noise}}{n_T}\right)^{1/2}\left(\frac{1+R^2}{1-R^2}\right)^{1/2}, \tag{27}$$

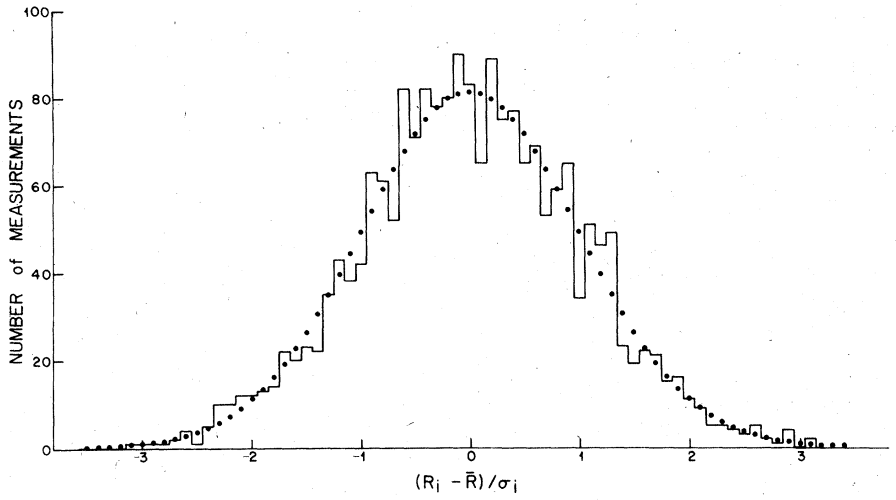

FIG. 4. Histogram for the distribution of the experimental data about the mean in units of the expected standard deviation for each point. The solid circles show the expected bar heights for a Gaussian distribution with the same mean and unit half-width.

where n_{noise}/n_T is the noise-to-signal ratio and F is the number of signal measurements between each noise measurement. Using $F=5$ and $n_{\text{noise}}/n_T=1/500$, the total theoretical standard deviation is

$$\sigma_{\text{tot}}=(\sigma_R^2+\sigma_{\text{noise}}^2)^{1/2}=0.000\,019\,9, \tag{28}$$

in statistical agreement with the experimental value. The standard deviation therefore shows no detectable fluctuations in the experimental results other than those arising from counting statistics. This conclusion is further supported by Fig. 4, which compares the histogram of the experimental data distribution about the mean (in units of the expected standard deviation for each point) with the theoretically expected histogram for a Gaussian distribution. The chi-square test of the fit, with the mean as the only adjustable parameter, yields $\chi^2=48.2$ for 49 degrees of freedom. Therefore, one could expect worse agreement about half the time.

One can also look for systematic variations in the data by means of runs tests. A high (low) run is defined to be a sequence of consecutive measurements which all fall above (below) the mean. The length of a run is simply the total number of elements contained in the sequence from beginning to end. The number of runs of a given length is asymptotically normally distributed. If n measurements are drawn from a random population with probability e_1 of falling above the mean and probability e_2 of falling below the mean ($e_1+e_2=1$), then the expected number of high runs of length i is asymptotically[20]

$$s_{1i}=ne_1^ie_2^2 \tag{29}$$

with variance

$$\sigma_{1i}^2=n\{e_1^{2i-1}e_2^3[(i+1)^2e_1e_2 - i^2e_2-2e_1]+e_1^ie_2^2\}. \tag{30}$$

The observed numbers of runs are compared with the expected numbers in Table II assuming that the measurements are drawn from a symmetric distribution so that $e_1=e_2=0.5$. Of the 2038 individual measurements, 49.0% fell above the mean and 51.0% fell below the mean. This is consistent with the expected fraction for a symmetric distribution of (50.0 ± 1.1)% on each side. With the exception of one unusually long low run, the results in Table II are in reasonable agreement with the expected numbers of runs. This appears to be a valuable test for systematic variations in long sequences of repeated measurements.

TABLE II. Comparison of observed numbers of low and high runs with the expected numbers of runs.

Run length	Low runs	High runs	Expected number
1	245	254	255 ±14
2	133	131	127 ±10
3	60	61	64 ± 7
4	33	33	32 ± 5
5	21	13	16 ± 4
6	7	5	8.0 ± 2.7
7	1	7	4.0 ± 1.9
8	2	2	2.0 ± 1.4
9	0	1	1.0 ± 1.0
10	1	0	0.5 ± 0.7
11	2	0	0.25 ± 0.5
12	0	0	0.12 ± 0.35
13	0	0	0.06 ± 0.25
14	1	0	0.03 ± 0.18
Total	506	507	510 ±11

V. SYSTEMATIC CORRECTIONS

The two systematic effects to be accounted for are the finite solid angle of observation of the detectors and the electronic dead time of the counting system.

The solid-angle effect is obtained by integrating the intensity as a function of direction over the source, and over the solid angle observed through the slit system shown in Fig. 4 for each point in the source. The intensity function is[21]

$$I(\theta)=A(1-\cos^2\theta)+A'(1+\cos^2\theta), \tag{31}$$

where A and A' are constants, and θ is the angle between the direction of observation and the electric field direction. Equation (23) can then be rewritten

$$R=(A'-A)/(3A'+A) \tag{32}$$

and the correction factor for the observed value R_{obs} can be expanded as

$$R=R_{obs}\left(1+(1-R)\frac{(\alpha^2+\beta^2)}{12(b-a)^2}+\frac{\gamma^2}{6b^2}+\frac{\delta^2}{8b^2}\right) \tag{33}$$

up to second order in the corrections. Here, a, b, α, and β are as shown in Fig. 5, γ is the slit height, and δ is the beam diameter. Corrections for the off-axis field inhomogeneity due to the quadrupole geometry do not enter until fourth order, and are therefore negligibly small. Using the values

$\alpha = 0.3810 \pm 0.0012$ cm,

$\beta = 0.4445 \pm 0.0012$ cm,

$\gamma = 0.5639 \pm 0.0012$ cm,

$\delta = 0.152 \pm 0.012$ cm,

$a = 4.826 \pm 0.001$ cm,

$b = 10.922 \pm 0.001$ cm,

the correction factor in (33) is 1.001 107 with an uncertainty of ±5 ppm. The dominant uncertainty is in the determination of the beam diameter δ.

The electronic dead time was estimated by measuring directly the duration of the pulses fed from the preamplifiers into the rate-meter counting system. Since the rest of the counting system was substantially faster, this should give a reasonable estimate. If the dead time is τ and the count rate is n/T, then to a first approximation the fractional loss of counts due to dead-time effects is

$$\delta n/n=\tau n/T \tag{34}$$

and the fractional decrease in R is

$$\delta R/R=\tfrac{1}{2}\tau\langle n/T\rangle(1-R^2), \tag{35}$$

where $\langle n/T\rangle$ is the total count rate for both counters averaged over a complete measurement. For our values of $\tau=(3\pm1)\times10^{-8}$ sec and $\langle n/T\rangle = 5.4\times10^3$ sec^{-1}, the fractional correction is $\delta R/R=(7.9\pm2.6)\times10^{-5}$. The uncertainty of 26 ppm is the largest source of error other than counting statistics.

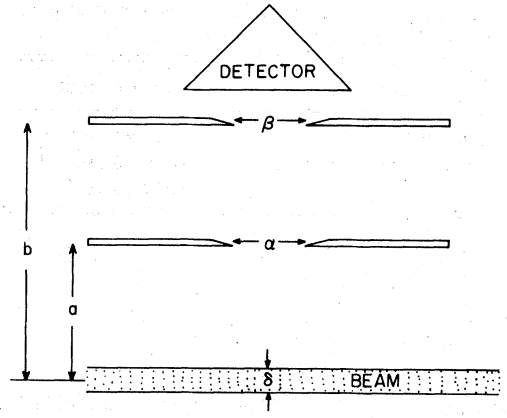

FIG. 5. Schematic diagram of the detector slit system. The dimensions are given in the text.

VI. RESULTS AND DISCUSSION

The final experimental value corrected for the finite solid angle of observation and electronic dead time is $R = 0.144\,259 \pm 0.000\,021$ (one standard deviation) in agreement with the theoretical value 0.144 245 calculated from the data shown in Table I. The various sources of error which contribute to the uncertainty of ±143 ppm are summarized in Table III. A number of other effects, such as background magnetic fields, beam contamination by hydrogen, and relativistic effects, were carefully considered and found to be negligible.

If one assumes that the other data in Table I are correct, then the measured R value corresponds to a Lamb shift of 1059.36 ± 0.16 MHz (70% confidence level). This value is compared with other experimental and theoretical determinations in Table IV. Our value agrees with the measurement of Cosens,[13] but disagrees by two standard deviations with the earlier measurement of Triebwasser *et al.*[11]

TABLE III. Sources of error in the measurement of R due to uncertainties in various parameters.

Parameter	$\delta R/R$ (ppm)
Counting statistics	138
Dead-time correction	26
Electric field strength	24
Fringing field effects	8
Solid-angle correction	5
$(\sum_i \delta R_i^2)^{1/2}/R$	143

TABLE IV. Comparison of theoretical and experimental Lamb shifts (MHz) in deuterium.

Theory	Experiment
1059.271 ± 0.025 [a]	1059.24 ± 0.06 [c]
1059.241 ± 0.027 [b]	1059.00 ± 0.06 [d]
	1059.36 ± 0.16 [e]

[a] Erickson, Ref. 22.
[b] Mohr, Ref. 23.
[c] Cosens, Ref. 13.
[d] Triebwasser, Ref. 11.
[e] Present work.

Although the present experiment is about a factor of 2.7 less precise than the measurements of Treibwasser *et al.*[11] and of Cosens,[13] further substantial improvements should be possible. Of the sources of error listed in Table III, the dominant one due to counting statistics can be reduced simply by counting longer and/or faster. The difficulty with counting faster is that the dead-time correction, and its associated uncertainty, become larger. The dead time was estimated only roughly in the present work (±30%), and a more accurate determination (or faster electronics) will be necessary if a higher-precision experiment is attempted. The estimated error arising from the electric field calculation comes primarily from the ±0.005 mm uncertainty in the diameters of the quadrupole rods. More accurately machined rods are now available, which would reduce the uncertainty in R from this source by about a factor of 2. An experiment at the 20 ppm level of accuracy should, therefore, be feasible.

For analogous experiments on heavier hydrogenic ions, the R values would lie much closer to the zero field values at the field strengths one would conveniently use, making the electric field determination and fringing field effects less important. Also, the numerical integration of the time-dependent Schrödinger equation becomes unnecessary—one can safely assume adiabatic entry. Specifically, the ratio of the quench rate for a hydrogenic ion of nuclear charge Z to the quench rate for deuterium is approximately $Z^2(E_Z/E_D)^2(\mathcal{S}_D/\mathcal{S}_Z)^2$, where E_Z/E_D is the ratio of electric field strengths in the two cases and $\mathcal{S}_D/\mathcal{S}_Z$ is the ratio of Lamb shifts. Thus, the same quench rate for deuterium obtained at 80 V/cm in the present work would occur at about 500 V/cm for He^+ and about 20 kV/cm for O^{7+}. The latter value is still within the range of field strengths that can be conveniently produced in the laboratory with the electrostatic quadrupole geometry. On the other hand, the finite electric field corrections to R arising from higher-order perturbation effects decrease in proportion to $1/Z^4$ along the isoelectronic sequence when the electric field strength is adjusted as shown above to keep the quench rate constant.

The only major new problem one encounters for the heavier hydrogenic systems is a false asymmetry, which appears when electrons produced by collisions with the background gas are accelerated by the quenching field into the detectors. This effect can be suppressed by the application of a small axial magnetic field to deflect the electron trajectories. The quadrupole geometry is an advantage in this regard because the off-axis electric field inhomogeneity helps to magnify the deflection. The required magnetic field strength of about 100 G for O^{7+} at a quenching field of 20 kV/cm is sufficiently small so as to make the magnetic field correction to the measurements negligible. Anisotropy measurements on He^+ and O^{7+} are in progress.

Note added in proof. It has recently been pointed out[24,25] that additional intensity asymmetries of measurable size may be present for the heavier hydrogenic ions due to interference between induced $E1$ and spontaneous $M1$ transitions to the ground state. For unpolarized beams,[24] the asymmetry is with respect to mirror reflections in the plane perpendicular to the electric field direction. However, the effect averages to zero if both directions are counted, and hence does not influence the present results.

ACKNOWLEDGMENT

Research support by the National Research Council of Canada and by a NATO travel grant is gratefully acknowledged.

[1] G. W. F. Drake, P. S. Farago, and A. van Wijngaarden, Phys. Rev. A 11, 1621 (1975).
[2] G. W. F. Drake and R. B. Grimley, Phys. Rev. A 8, 157 (1973).
[3] C. Y. Fan. M. Garcia-Munoz, and I. A. Sellin, Phys. Rev. 161, 6 (1967).
[4] H. W. Kugel, M. Leventhal, and D. E. Murnick, Phys. Rev. A 6, 1306 (1972).
[5] M. Leventhal, D. E. Murnick, and H. W. Kugel, Phys. Rev. Lett. 28, 1609 (1972).
[6] G. P. Lawrence, C. Y. Fan and S. Bashkin, Phys. Rev. Lett. 28, 1613 (1972).
[7] H. Gould and R. Marrus, in *Abstracts of the Fifth International Conference on Atomic Physics*, edited by R. Marrus, M. Prior, and H. A. Shugart (University of California, Berkeley, 1976), p. 207.
[8] M. Leventhal, Phys. Rev. A 11, 427 (1975).
[9] H. W. Kugel, M. Leventhal, D. E. Murnick, C. K. N.

Patel, and O. R. Wood, II, Phys. Rev. Lett. 35, 647 (1975).
[10]H. W. Kugel and D. E. Murnick, Rep. Prog. Phys. 40, 297 (1977).
[11]S. Triebwasser, E. S. Dayhoff, and W. E. Lamb, Jr., Phys. Rev. 89, 98 (1953).
[12]R. T. Robiscoe, Phys. Rev. 168, 4 (1968).
[13]B. L. Cosens, Phys. Rev. 173, 49 (1968).
[14]E. Lipworth and R. Novick, Phys. Rev. 108, 1434 (1957); M. A. Narasimham and R. L. Strombotne, Phys. Rev. A 4, 14 (1971).
[15]S. R. Lundeen and F. M. Pipkin, Phys. Rev. Lett. 34, 1368 (1975).
[16]D. D. McCracken and W. S. Dorn, *Numerical Methods and Fortran Programming* (Wiley, New York, 1964), p. 377.
[17]E. J. Kelsey and J. Macek, Phys. Rev. A 16, 1322 (1977).
[18]G. W. F. Drake, J. Phys. B 10, 775 (1977).
[19]Equation (26) is equivalent to Eq. (28) of Ref. 1 for $\alpha = 1$.
[20]A. M. Mood, Ann. Math. Stat. 11, 367 (1940).
[21]G. W. F. Drake and C-P. Lin, Phys. Rev. A 14, 1296 (1976).
[22]G. W. Erickson, Phys. Rev. Lett. 27, 780 (1971).
[23]P. J. Mohr, *Beam Foil Spectroscopy*, edited by I. A. Sellin and D. J. Pegg (Plenum, New York, 1976), p. 89.
[24]P. J. Mohr, Bull. Am. Phys. Soc. 22, 1314 (1977) and Phys. Rev. Lett. (to be published).
[25]G. W. F. Drake, Phys. Rev. Lett. (to be published).